A Comparison of Measured and Wind-derived Ekman Transport at 11°N in the Atlantic Ocean

T. K. CHERESKIN AND D. ROEMMICH

Scripps Institution of Oceanography, La Jolla, California

(Manuscript received 11 June 1990, in final form 2 January 1991)

ABSTRACT

A comparison of measured and wind-derived ageostrophic transport is presented from a zonal transect spanning the Atlantic Ocean along 11°N. The transport per unit depth shows a striking surface maximum that decays to nearly zero at a depth of approximately 100 m. We identify this flow in the upper 100 m as the Ekman transport. The sustained values of wind stress and the penetration depth of the Ekman transport reported here are considerably greater than in previous observations, which were made in conditions of light winds. The transport of $12.0 \pm 5.5 \times 10^6$ m^3 s^{-1}, calculated from the difference of geostrophic shear and shear measured by an acoustic Doppler current profiler, is in good agreement with that estimated from the shipboard winds, $8.8 \pm 1.9 \times 10^6$ m^3 s^{-1}, and from climatology, $13.5 \pm 0.3 \times 10^6$ m^3 s^{-1}. Qualitatively, the horizontal distribution of the wind-driven flow was best predicted by the shipboard winds. The cumulative transport increased linearly over the western three-fourths of the basin, where the winds were large and spatially uniform, and remained constant over the eastern fourth where the easterly stress was uncharacteristically low. The mean depth of the Ekman transport extended below the mixed layer depth, which varied from 25 to 90 m. The profile of ageostrophic transport does not appear consonant with slablike behavior in the mixed layer, even when spatial variations in mixed layer depth are taken into account.

1. Introduction

One of the oldest theories of wind-driven ocean circulation is that of Ekman (1905), who proposed a balance of forces in the surface layer between a steady wind stress and the Coriolis force, resulting in an anticyclonic velocity spiral and a net surface layer transport at right angles to the wind direction. Although Ekman's theory was motivated by F. Nansen's observations of ice drifting at an angle to the wind, subsequent quantitative testing of the theory has proven very difficult. Two direct tests of the Ekman transport relation have been carried out using moored measurements of winds and ocean currents at midocean locations. Davis et al. (1981) calculated a transport to the right of the wind which was 20% to 40% lower than the predicted value at Station P in the northeastern Pacific. The discrepancy was attributed to either overestimation of the wind stress, underestimation of current, or momentum loss due to wind waves. The Ekman transport extended to about 30 m depth, which was the maximum mixed layer depth seen during the experiment. Price et al. (1987) reported agreement between measured and predicted transport to within about 10%, under low wind conditions in the Sargasso Sea. Again the Ekman transport was confined to the mixed layer above about 25 m.

In addition to the direct tests of the Ekman transport relation, several indirect or consistency tests have also been made. In the equatorial band and in regions of coastal upwelling, the wind-driven surface flow is divergent, with geostrophic convergence thought to balance the mass budget of the upper layers. Agreement between geostrophic convergence calculated from hydrographic data and Ekman divergence calculated from climatological wind stress has been found by Wyrtki (1981) in the equatorial Pacific, Roemmich (1983) in the equatorial Atlantic, and Roemmich (1989) in the coastal zone off southern California. In each case the geostrophic convergences occurred in the upper few hundred meters.

These direct and indirect calculations leave several unanswered questions for which additional measurements of ocean currents and winds are required. First and perhaps most obvious is the question of the accuracy of estimates of Ekman transport calculated from the wind in a variety of locations and wind conditions. Instrumental errors, sampling errors, errors in the drag coefficient, and deviations from the assumed momentum balance may all cause significant discrepancies. Additional measurements are also required for questions relating to the vertical structure of the wind-driven flow: What is the vertical distribution of the Ekman

Corresponding author address: Dr. Teresa Chereskin, University of California, San Diego, Scripps Institution of Oceanography, 0230, La Jolla, CA 92093.

transport? Does it extend below the mixed layer? How does the vertical distribution of mass transport affect the wind-driven fluxes of heat and salt? The questions are important ones. Studies of net meridional transport in the oceans show that the Ekman transport is an important component of the mass budget of the upper layers at most latitudes and in most oceans. In the tropics meridional Ekman transport driven by the easterly Trades can exceed 10–20 Sv ($1\ \text{Sv} \equiv 10^6\ \text{m}^3\ \text{s}^{-1}$) when added up over the width of an ocean basin and may dominate the warm water budget and consequently the meridional heat transport of these regions.

Here we address the above questions using a combination of hydrographic data, acoustic Doppler current profiler (ADCP) data, and shipboard wind observations made during March 1989 along 11°N in the Atlantic Ocean. These data are described in section 2. Section 3 presents three estimates of Ekman transport: an estimate based on ageostrophic velocity estimates, an estimate based on in situ wind measurements, and an estimate based on wind climatology. The vertical and horizontal distribution of the Ekman transport is discussed in section 4, followed by conclusions in section 5. The errors in the transport estimates are presented in an appendix.

2. Description of data

In March 1989 the R/V *Oceanus* completed a transect from Senegal to French Guiana, collecting CTD, hydrographic, ADCP, and wind measurements. Figure 1 shows the positions of 84 CTD stations, with measurements made from the ocean surface to within 10 m of the bottom. The length of the track is approximately 4000 km, with average midocean station spacing of 60 km and shorter spacing near the coasts. The first and last stations were near the 200 m isobath; the water depth for all other stations was greater than 500 m.

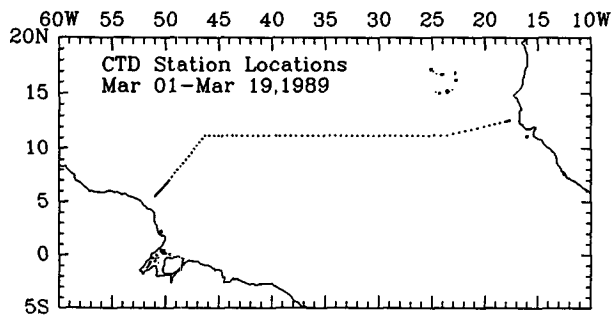

FIG. 1. Locations of 84 CTD stations, occupied by R/V *Oceanus*, in March 1989. Station 1 was near the 200 m isobath off Senegal (12.6°N, 17.6°W) on 1 March. The ship angled southwestward for a short segment, then steamed due west along 11.2°N. A second course change to the southwest was made in order to approach the South American coast perpendicularly. Station 84 was near the 200 m isobath off French Guiana (5.5°N, 51°W) on 19 March. For purposes of discussion, station 84 is considered the origin of the ship track, with distance increasing towards the east.

In February 1989, on the previous *Oceanus* leg, an array of 29 SOFAR floats was deployed by P. Richardson and W. Schmitz along a nearly identical ship track to that occupied in March. The float transect began off French Guiana and ended about 500 km off Senegal, at which point the ship deadheaded due north to the Canary Islands. For the purpose of discussion in this paper, the February leg will be referred to as leg 1, and the March leg will be referred to as leg 2. Along-track distance increases from west to east for both legs, and the track origin is at 5.5°N, 51°W. Weather observations were made on both legs; all other observations discussed in this paper were made on leg 2 only.

Instantaneous ship speed, ship heading, wind speed, and wind heading were sampled every 5 minutes. East and north components of wind velocity relative to the ship were calculated, then the east and north components of ship velocity were removed to yield absolute wind velocity. Beaufort scale wind observations were made every 4 hours by the bridge on both legs. Although less accurate than the measured wind, the Beaufort observations provide some measure of the temporal variability of the observed wind field from February to March 1989. They are used qualitatively in the next section when the directly measured winds are compared to the Hellerman and Rosenstein (1983) March climatological mean. The closest repeat observation of Beaufort scale winds was at 3500 km along the ship track, separated by approximately 2 weeks.

The *Oceanus* shipboard ADCP was an RD Instruments (RDI) 153.6 kHz hull-mounted profiler consisting of four transducers directed downward 60° from horizontal and equally spaced in azimuth. The acoustic pulse length was 25.12 ms and the bin length was 6.28 ms, corresponding to nominal vertical intervals of 16.75 and 4.2 m, respectively, using a sound speed of 1540 m s^{-1}. The sound speed was calculated from measured temperature and salinity at the transducer depth (5 m). The recorded east and north velocities were averaged over 150 s intervals, or about 90 pings. The shallowest reliable measurement was at 25.8 m, and the deepest was at approximately 300 m. The mean sound speed profile calculated from the CTD measurements was used to calculate the ADCP measurement depths. Although the *Oceanus* GPS receiver was not working during the cruise, two GPS receivers were obtained at the end of the cruise for the purpose of calibrating the ADCP transducer misalignment. The angle correction was determined using four satellite GPS navigation and ADCP bottom tracking in shallow water (Pollard and Read 1989). The scale factor correction that was determined from the GPS calibration data agreed with that calculated using the ratio of the in situ sound speed to the RDI default sound speed of 1500 m s^{-1}.

3. Estimates of Ekman transport

a. An estimate based on ageostrophic velocity

Both the ADCP and the hydrographic data provide measures of current shear rather than absolute current. The geostrophic shear can be estimated from the hydrographic data while the total shear (geostrophic plus ageostrophic components) is measured by the ADCP. The ageostrophic flow is expected to be surface-trapped. Here we will assume that the flow at 250 m, far below the base of the mixed layer, is in geostrophic balance. Then the difference between ADCP velocity and geostrophic velocity, using 250 m as a reference level in both cases, is equal to the absolute ageostrophic velocity. To reiterate, our assumption is not that the velocity vanishes at 250 m but that the ageostrophic component of velocity vanishes at that depth. This distinction is critical.

Geostrophic currents were calculated between each CTD station pair. The net relative geostrophic transport is southward, a result one can anticipate by noting that the isotherms in the upper 200 m have a net downward displacement from east to west (Figs. 2a, 2b). The across-track ADCP velocities were averaged over the same CTD station-pair intervals and the differences calculated (Figs. 2c, 2d).

A strong northwestward flow is apparent at the western boundary of the transect, near 51°W, in both the geostrophic and the ADCP velocities relative to 250 m. This flow was observed to be of order 1 m s^{-1} on the wide shallow shelf off French Guiana (not shown) using the ADCP in bottom tracking mode. A broad dome in the isotherms, centered between 48° and 49°W, extended a kilometer in depth and indicates a geostrophic eddy or flow/counterflow that is also apparent in the geostrophic and ADCP velocities (and therefore not in the ageostrophic velocity). The most striking ageostrophic features are the northward velocity maximum located near 44°W at a depth of 150 m, and a shallower southward maximum located at 40.5°W (Fig. 2d). These maxima may be due to near-inertial internal waves. Although we cannot determine the source from these measurements, the ubiquity of a near-inertial peak in internal wave spectra, together with continuous wind forcing, guarantees the presence of such waves. The velocity in the eastern half of the transect was smaller and less vertically sheared than that in the western half. The winds along the African coast were upwelling favorable, and the isotherms are bowed up near the coast. Isotherm spreading at the eastern boundary, centered at 150 m, indicates a poleward undercurrent.

Figure 3 shows the transport per unit depth, integrated across the basin. The net ageostrophic transport is northward, with a large near-surface maximum which we identify as the wind-driven component. This component decays with depth and extends to approximately 100 m. Below the wind-driven transport, there is a secondary maximum of small vertical scale peaked at 150 m, arising from the velocity feature near 44°W. The ageostrophic transport in the upper 20 m was estimated by linear extrapolation from the calculated values at 30–50 m. Total ageostrophic transport above 100 m is 12.0 ± 5.5 Sv. Derivation of the error bar is discussed in the Appendix. Because of the large vertical extent of the wind-driven ageostrophic transport, the uncertainty in the surface extrapolation introduced a relatively small (less than 10%) error in the net transport (the difference between a slab and a linear extrapolation).

b. Estimates based on wind stress

East and north components of wind velocity were averaged over the intervals between CTD stations. The east (τ_x) and north (τ_y) wind stress components were

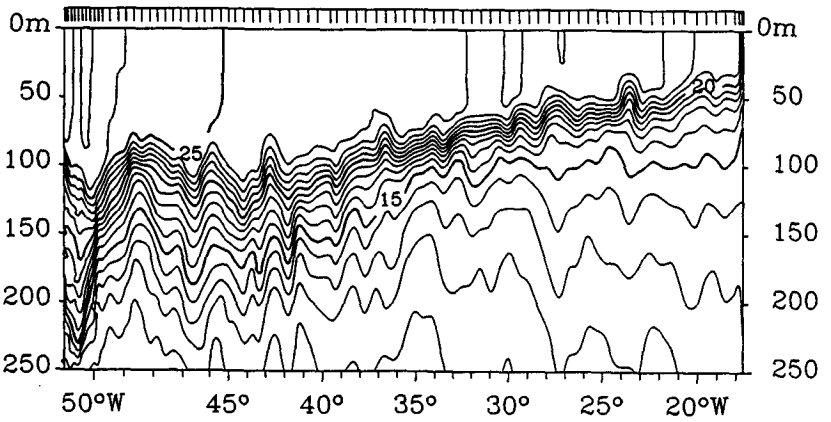

FIG. 2a. Vertical section of temperature (°C) from Senegal (on the right) to French Guiana. Tics on top axis mark location of CTD stations. Along-track distance and location of ship course changes are shown on scale of Fig. 2d.

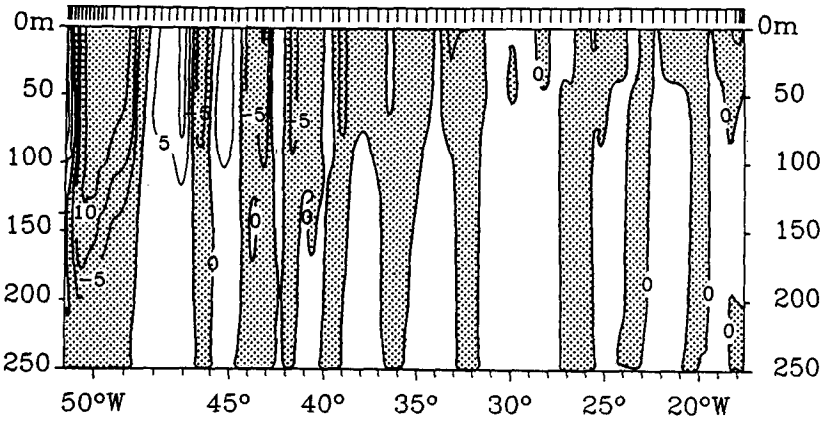

FIG. 2b. Vertical section of geostrophic velocity (cm s^{-1}) relative to 250 m. Regions of southward flow are shaded.

computed using the bulk formulas given by Large and Pond (1981). The east (M_x) and north (M_y) transports were computed using the Ekman transport relation:

$$M_x = \frac{\tau_y}{f\rho_w}; \quad M_y = \frac{-\tau_x}{f\rho_w}$$

where f is the Coriolis parameter and the water density $\rho_w = 1025$ kg m^{-3}. The along-track components of the measured wind stress are shown in Fig. 4a. Hellerman and Rosenstein (1983, hereafter referred to as HR) mean monthly stress for March is shown for comparison. The wind-derived estimate of Ekman transport was 8.8 ± 1.9 Sv from in situ wind observations, and 13.5 ± 0.3 Sv from HR mean monthly winds for March.

The estimated along-track stress was less than the HR climatological mean for the entire section. Part of this difference may have been due to HR's use of a drag coefficient which is about 20% higher than Large and Pond's (1981) value for winds of 4 to 11 m s^{-1} and neutral stability. Large differences from the HR climatology occur in two regions: in the western Atlantic from 250 to 750 km and in the eastern Atlantic from 3000 to 4000 km. In particular, the anomalous stress in the eastern basin was near-zero, implying zero across-track transport, and persisted over 1000 km and 5 days of transit.

The Beaufort scale observations from both cruise legs were converted to wind speed using the new Beaufort equivalent scale (Kaufeld 1981). The wind speeds were then interpolated to the CTD station spacing, and wind stress and transport were computed in the same manner as for the directly measured winds. For leg 1, wind speed from 3500 to 4000 km was extrapolated using the mean value from 3000 to 3500 km. The resolution of the Beaufort scale estimates is much coarser, both spatially and in the actual speed estimates. The wind observations were in the range 2–7 Beaufort. The revised scale yields higher speeds than the old scale in the range 1–6 Beaufort and lower speeds in the range 10–12 Beaufort.

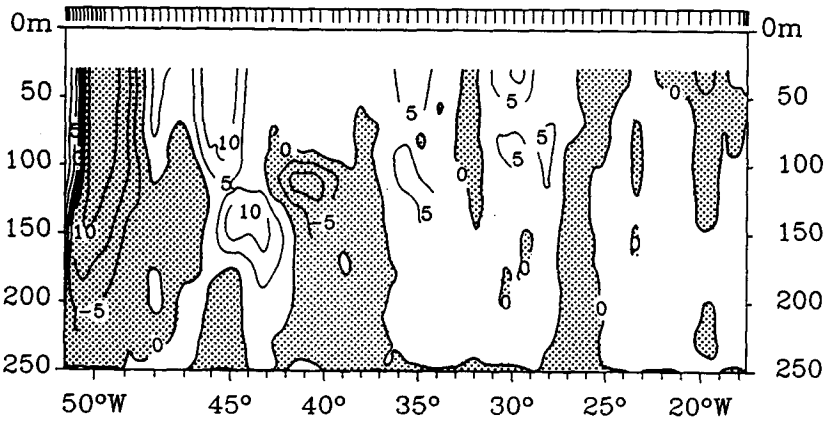

FIG. 2c. Vertical section of across-track component of ADCP velocity (cm s^{-1}) relative to 250 m. Regions of southward flow are shaded.

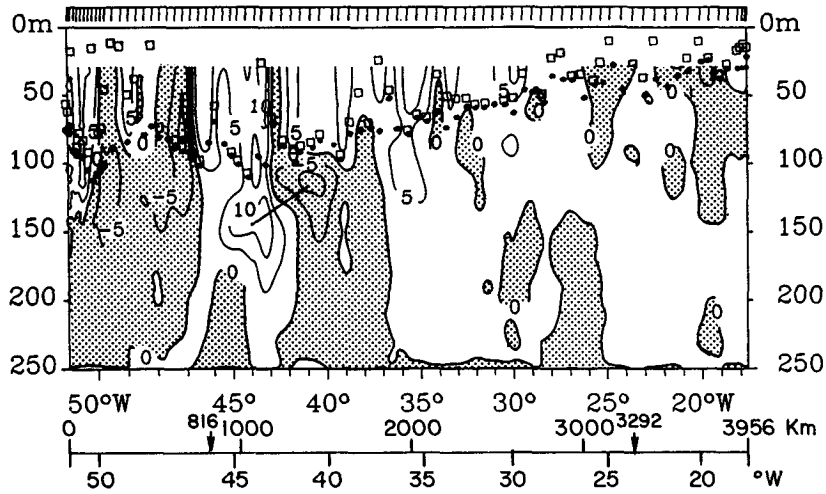

FIG. 2d. Vertical section of smoothed difference, ADCP − geostrophic velocity, i.e., ageostrophic velocity relative to 250 m. Regions of negative velocity difference are shaded. Solid (open) symbols denote the depth where the temperature is 1.0 (0.1) °C cooler than the temperature at 6 m. The sloping line connecting the velocity maxima between 40° and 45°W suggests a vertically propagating wave. The ship course changes noted in Fig. 1 are marked by the arrows at 816 and 3292 km on the distance scale.

Comparing the wind stress estimated from Beaufort wind velocities to that estimated from the measured wind velocities from leg 2 showed that the Beaufort estimates were biased high relative to the measured winds (Fig. 4a). However, the pattern of spatial variation of both sets of wind observations from leg 2 was nearly identical. In particular, both indicated the presence of a near-zero along-track component of stress from 3000–4000 km along the cruise track of leg 2. A comparison of the Beaufort wind estimates from the consecutive cruise legs indicated that this region of low along-track wind stress was not present during the leg 1 observations made 2 weeks earlier (Fig. 4b).

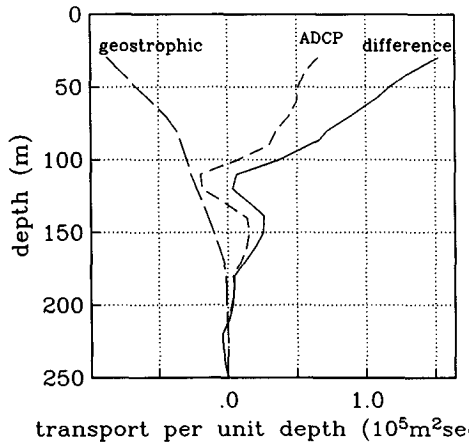

FIG. 3. Basin-integrated transport per unit depth (10^5 m^2 s^{-1}). Solid curve is the ageostrophic transport (ADCP − geostrophic). Large dashed curve is geostrophic transport; small dashed curve is ADCP transport.

Using the Beaufort estimates, the wind-derived transport was 24.8 Sv from leg 1 and 14.5 Sv from leg 2. Part of the decrease in transport is due to the decrease in along-track wind stress in the eastern fourth of the basin. However, bias errors such as a correlation between wind estimation and the direction of steaming with respect to the wind may influence these estimates. Leg 1, on which consistently higher wind speed estimates were made, was steamed into the wind with little station time. Leg 2 was steamed with following seas and about 50% station time. Hence, the chief conclusion that we draw from these estimates is that the large-scale wind field was not stationary over time periods of 2 weeks and more.

4. Discussion

In this section the vertical and horizontal distributions of the Ekman transport are considered, as well as the nature of the variability. Principal questions are whether the ageostrophic flow within the mixed layer is sheared or slablike and whether it penetrates below the base of the mixed layer. Complications arise from the large change in the thickness of the mixed layer between the eastern and western tropical Atlantic (Fig. 2a) and from ambiguity in defining the mixed layer.

Previous attempts to estimate the Ekman penetration depth by fitting velocity observations to an Ekman spiral (Weller 1981; Price et al. 1987) were inconclusive because the vertical scale of amplitude decay did not match the vertical scale of spiralling. Davis et al. (1981) found no evidence of spiralling in the Ekman layer in the MILE experiment. There the response was consonant with a slab model of the mixed layer, and the

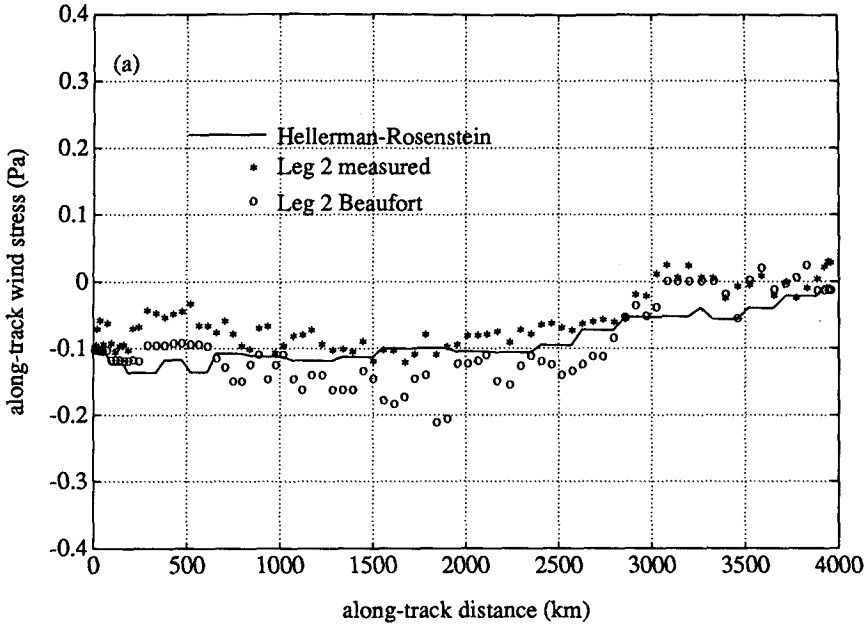

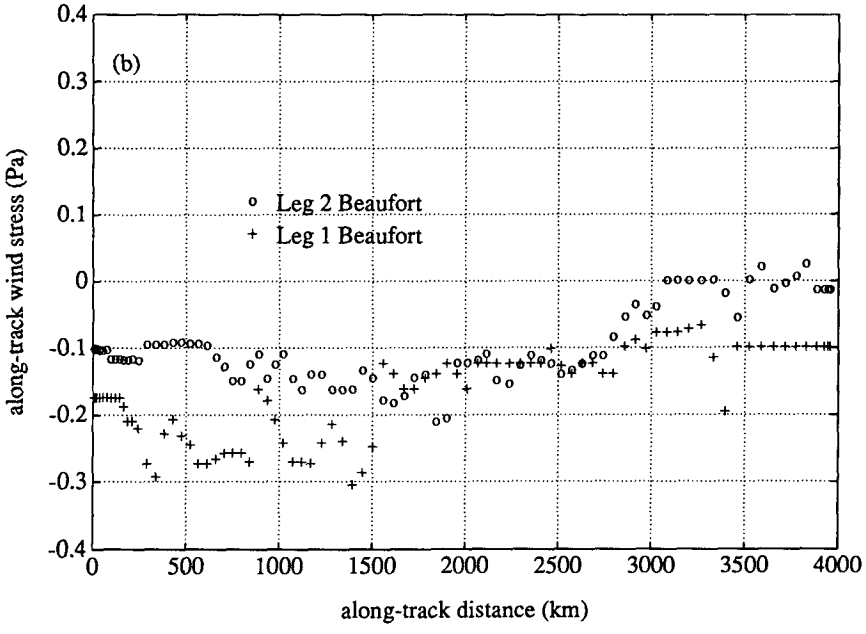

FIG. 4a. Comparison of shipboard measured wind stress (*), and Beaufort wind stress (O) during March 1989, and Hellerman and Rosenstein climatological mean March wind stress (solid line) along the ship track (Senegal is on the right). Units are pascals.

FIG. 4b. Comparison of Beaufort wind stress from February 1989, leg 1 (+) and Beaufort wind stress from March 1989, leg 2 (O). Units are pascals.

observed shear in the mean profile could be explained by temporal variations in the mixed layer depth.

In analogy with the result of Davis et al. (1981), one might suppose that shear in the profile of ageostrophic transport for the Atlantic transect (Fig. 3) could be the result of a slablike response in the mixed layer, but with large variations in mixed layer depth across the basin causing the apparent shear. To test this, depth was normalized at each station pair by the local mixed layer depth; then, the transport was calculated for each interval of one-tenth of the mixed layer depth. Thus, if the mixed layer depth was 90 m at a

particular station pair, we would calculate the transport in each 9 m interval—5 m intervals for a 50 m mixed layer and so on. Results from all station pairs were then added to form the basinwide estimate (Fig. 5). Since the null hypothesis here is of a slablike response, we have set the velocity at 0–20 m (above the depth range seen by the ADCP) equal to the velocity at 30 m. The two curves of Fig. 5 represent two different definitions of mixed layer depth. The base of the mixed layer is defined as the depth where the temperature is 1.0°C (solid line) or 0.1°C (dashed line) cooler than the temperature at 6 m—which is below the depth of diurnal influence in our measurements. These two will be referred to as the mixed layer depth (MLD) and the well-mixed layer depth (WMLD) respectively.

For a perfect slablike response, Fig. 5 would show a vertical line (no shear) down to 1.0 times the mixed layer depth, dropping abruptly to zero at that point. Neither line in Fig. 5 appears at all slablike. The vertical segment at the top of each line is due to the assumption of no shear above 30 m. Below this, the transport profiles drop off approximately linearly, to near zero at about 1.2 normalized depth units in the MLD case and nearly 2 in the WMLD case.

The MLD and the WMLD have been displayed in Fig. 2d in order to show the variations across the width of the basin. At some locations the two are nearly equal while elsewhere the surface layer has become weakly stratified and the WMLD is very shallow. There is much more high frequency variability in the WMLD. Nevertheless, it is fairly clear that no choice of definition for the mixed layer will produce a slablike appearance in Fig. 5. While one might further tighten the definition beyond that of the WMLD case, and in so doing reduce the shear between 0 and 1 normalized depth units, the tradeoff is that the ageostrophic shear will then extend even deeper in terms of the normalized depth. Given the ambiguous nature of the depth normalization (Fig. 5), we feel that the Ekman transport has best been defined by the (unscaled) depth where the basin-averaged ageostrophic transport approaches zero, i.e., 100 m (Fig. 3, Table 1). The penetration of ageostrophic transport below the base of the mixed layer has a significant implication for basinwide estimates of the Ekman heat transport. The transport weighted average temperature above 100 m is about one degree cooler than the surface temperature.

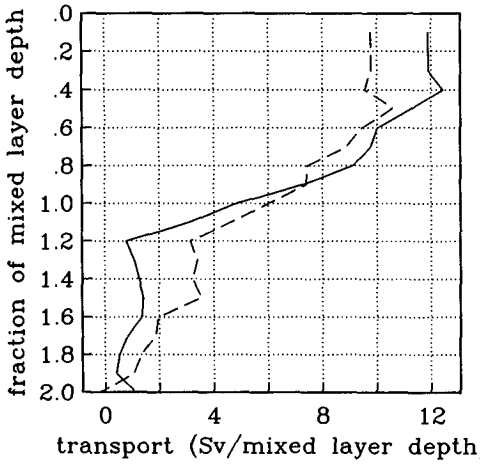

FIG. 5. Basin-integrated transport per unit of mixed layer depth (10^6 m^3 s^{-1}). The mixed layer depth for the solid (dashed) curve is defined as the depth where the temperature is 1.0 (0.1) °C cooler than the temperature at 6 m. Velocity at 0–20 m was set equal to velocity at 30 m (slab extrapolation). Vertical coordinate is fraction of mixed layer depth.

The horizontal distribution of wind-derived transport (dashed curves) and of ageostrophic transport integrated to the WMLD, the MLD, and 100 m (solid curves) are compared in Fig. 6. The cumulative transport based on the climatological March wind increases over the entire basin, unlike the transport estimates made for March 1989. Although station pair estimates of ageostrophic transport are noisy, the cumulative transport integrated across the basin shows a robust trend, increasingly nearly linearly across the western three-fourths of the basin and negligible transport in the eastern fourth, in agreement with the shipboard wind estimate. Fluctuations in the ageostrophic transport are on the order of 1 Sv. The main difference between the various 1989 estimates is in the rate of increase of the transport (slope) over the western three-fourths of the basin. The ageostrophic transport above the MLD gives a good overall fit to the in situ wind estimate, with a net ageostrophic transport that is nearly identical to the wind-derived estimate. Over the westernmost 1000 km, the three ageostrophic estimates are separated by almost fixed offsets. From 1000 to 3000 km, the transports accumulate at different rates, with larger rates of increase corresponding to deeper integration depths. The ageostrophic transport above 100 m increases at approximately 5 Sv per 1000 km, whereas the transport above the MLD increases at about 4 Sv per 1000 km. Note that the constant rate of accumulation for the transport above the MLD occurs despite the fact that the integration depth is decreasing approximately linearly. From 3000 to 4000 km all three estimates show negligible increase in transport. The largest difference in the transport estimates is apparent in midbasin, where the ageostrophic velocity is almost exclusively northward. The fact that the ageostrophic flow appeared to extend below the mixed layer (Fig. 5) led us to choose the flow above 100 m as the best estimate. However, with the large error bars in the calculations, the different estimates are indistinguishable. All of the estimates from wind stress and measured ageostrophic transport are summarized in Table 1.

Inertial oscillations in the mixed layer represent ageostrophic flow that is not part of the Ekman transport, and is therefore noise in the present instance.

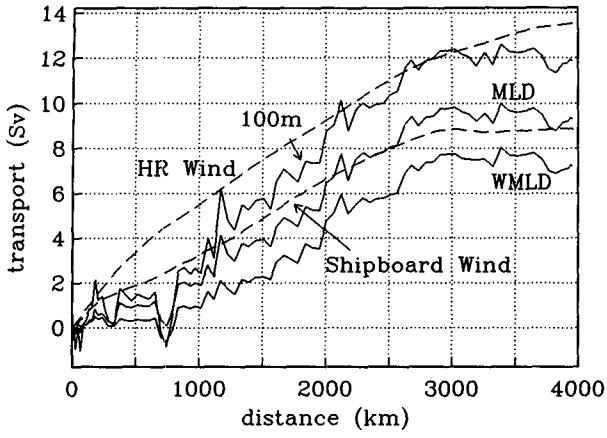

FIG. 6. Cumulative transport (10^6 m^2 s^{-1}) along the ship track (Senegal is on the right). Dashed curves represent the transport estimated from climatological (top) and shipboard (bottom) winds. Solid curves represent the transport estimated from ageostrophic velocity integrated to three depths (top to bottom): 100 m, the MLD, the WMLD.

Inertial oscillations are forced by variations in the wind field with time scales less than an inertial period (Pollard 1977). Only waves with frequencies within a few percent of f remain in the mixed layer for longer than an inertial period; at higher frequencies they radiate away. Since their angle of propagation with respect to the horizontal is small, near-inertial oscillations found a few tens of meters beneath the mixed layer are probably not locally generated and result from propagation. The oscillations within the mixed layer typically have small shear; however, they are associated with a large shear across the base of the mixed layer. Averaging over many inertial periods will remove the inertial oscillations at a fixed location. However, inertial oscillations are observed to be highly intermittent, in part due to variability in wind forcing. Because our spatial averaging includes a relatively small number of independent estimates, there is considerable residual noise.

In the eastern basin where the mixed layer was shallow and the wind forcing was weak, there was negligible shear throughout the top 250 m. In the western basin the mixed layer deepened to about 90 m, the wind forcing was strong, and we observed energetic, circularly polarized, relative currents of large horizontal coherence just below the base of the mixed layer. These are characteristic signatures of inertial motion (Leaman and Sanford 1975; D'Asaro 1984; Chereskin et al. 1989). Much of this variability was reduced by averaging. The energetic shear was on the order of 10^{-2} s^{-1}, while the shear within the mixed layer (but deeper than the shallowest sample bin at 26 m) was typically 1–2 orders of magnitude smaller.

For linear internal waves the frequency σ depends only on the angle of propagation with respect to the vertical. The previously noted velocity maxima in the ageostrophic velocity are suggestive of vertical propagation (Fig. 2d). Estimating a slope of order 10^{-4} and a calculated Brunt-Väisälä frequency $N = 0.02$ s^{-1}, we find $\sigma = 1.002f$, with a horizontal wavelength of order 700 km and a vertical wavelength of order 60 m.

The large-scale, spatially intermittent, ageostrophic currents that were present below the mixed layer may be near-inertial waves. The horizontal scales are consistent with the estimated wavelengths of such waves (Chereskin et al. 1989). Because of their large horizontal scale and amplitude (10 cm s^{-1}), and because of their intermittency, they contribute to the total ageostrophic transport (the secondary maximum at 150 m). Intermittent inertial flows within the mixed layer may also be present, and may be the source of the estimated variance in the basinwide total. The success of the Ekman transport calculation, in spite of substantial noise, is due to the persistent moderate wind stress of the trades, low latitude (small f) and deep mixed layer.

5. Conclusions

We have attempted to address a number of questions regarding the Ekman transport relation using shipboard measurements of upper ocean currents and wind stress averaged over a 4000 km transect of the tropical North Atlantic. The calculated profile of ageostrophic transport per unit depth shows a striking surface maximum that decays to a near-zero value at a depth of approximately 100 m. We identify this surface-connected maximum as the wind-driven transport. The sustained values of wind stress, mixed layer depth and penetration depth of the Ekman transport reported here are considerably greater than those reported by Davis et al. (1981) and Price et al. (1987). The directly estimated transport (12.0 ± 5.5 Sv) compares favorably with transport calculated from shipboard winds (8.8 ± 1.9 Sv) and transport estimated from the climatological monthly mean winds (13.5 ± 0.3 Sv). However, the error bar on our direct estimate is large, since it is based on a single transect. The observed spatial structure of transport across the basin is more robust than the error bar would suggest, with the estimated cumulative transport increasing linearly over the western three-fourths of the basin, corresponding to large and

TABLE 1. Estimates of Ekman transport (units are 10^6 m^3 s^{-1}).

Estimates based on ageostrophic velocity	
Integral to 100 m*	12.0 ± 5.5
Integral to MLD	9.3
Integral to WMLD	7.0
Estimates based on in-situ wind stress	
Measured wind, March 1989*	8.8 ± 1.9
Beaufort wind, March 1989	14.5
Beaufort wind, February 1989	24.8
Estimates based on climatological wind stress	
Hellerman-Rosenstein March mean*	13.5 ± 0.3

* Estimates with error bars are considered "best" estimates.

steady (i.e., spatially uniform) easterly winds, and negligible transport in the eastern quarter where the easterly stress was uncharacteristically low. Thus, the measured wind-driven transport showed better qualitative agreement with the in situ winds than with the climatological winds, although the value of the transport estimate fell between these two estimates. The mixed layer deepened markedly from about 25 m in the eastern basin to 90 m in the western basin, and the observed wind-driven currents extended below the mixed layer across most of the basin. Integration of the Ekman heat transport across the basin resulted in a value equivalent to using a constant temperature about 1° colder than the ocean surface temperature.

The close agreement of the transport values from all three calculations lend some confidence to our ability to extract the wind-driven currents from the observed current field. We expect the signal-to-noise ratio for this type of calculation to be high in regions of the ocean with large, steady wind forcing and deep mixed layers. The noise from inertial oscillations appears significant, and further averaging using repeated or longer sections would be required to reduce the noise level. The present calculation represents only a single realization across one Atlantic latitude. We hope that it is a useful prototype for similar calculations at other locations having different wind characteristics and mixed layer depths. Repeated transects or longer (i.e., larger basin) transects are required in order to improve the signal-to-noise ratio and to enable the horizontal structure of the wind-driven flow to be examined. Many long hydrographic sections are planned for the coming decade in a comprehensive effort to describe the large-scale circulation of the global oceans. The Ekman transport is an important component of the flow which merits a serious effort to obtain a high quality set of direct observations. While time-series observations similar to Davis et al. (1981) and Price et al. (1987) may ultimately provide the best statistical reliability, it is certainly desirable to make direct measurements of the Ekman transport a part of large-scale expeditions spanning the globe.

Acknowledgments. We thank Captain Palmieri and the crew of the R/V *Oceanus* for their excellent ship handling. The efforts of B. Walden to get a GPS receiver to Barbados were much appreciated. We thank S. Isakari for her help with the wind data, and P. Richardson and D. Moller for making available the *Oceanus* deck logs. This paper has benefitted from conversations with M. Hall and A. Harding. Support for this work was provided by NSF Grant OCE-8716314.

APPENDIX

Estimation of Errors

Error estimates given in the preceding sections are standard errors produced either by piecewise averaging along track in our single realization or averaging over many realizations in the case of wind stress climatology. The climatology is based on 106 years of observations, and the tropical Atlantic is relatively well sampled. The source of error in the geostrophic transport is identified below as variance in the transport at the eastern and western boundaries, while the source of error in the ADCP transport is identified as variance in the basin interior. The standard errors in the geostrophic and ADCP transports were computed in the boundary and interior regimes, respectively, by assuming that the transport within each regime is an ergodic random process, and therefore spatially averaged properties are equal to ensemble averaged properties.

The net ageostrophic transport T is the difference of between the ADCP and geostrophic transport integrals, with integration limits corresponding to penetration depth H (100 m) and the length L of the steaming track:

$$T = T^d - T^g = \int_0^L \int_{-H}^0 V^d dz dx - \int_0^L \int_{-H}^0 V^g dz dx$$

Transport and velocity are denoted by T and V, and ADCP and geostrophic quantities are denoted by superscripts d and g, respectively.

The vertical shear in geostrophic transport (e.g., Fig. 3, long dashed line) depends only on horizontal differences in density between the eastern and western ends of the transect. We assume that the error in this estimate is largely due to temporal changes in the density field during the 20 days of the transect and that it can be approximated from the spatial variations of the density field near the boundaries. Using 20 station pairs nearest the boundaries, with an average spacing of 30 km, the standard deviation of the transport in the upper 100 m was calculated and the error was estimated to be 1 Sv.

A complete examination of the sources of variance in the ADCP velocity estimates is not attempted here. However, much of the ping-to-ping variability in velocity estimates is random and is greatly reduced by averaging over a large number of pings. The source of this variability is due to the properties of the acoustic system and the scattering volume. The variance due to wave-induced ship motion is also greatly reduced by averaging (Kosro 1985). After averaging over one hour, the expected error is less than 1 cm s^{-1}. Absolute current estimates, using navigation to remove the ship speed, are sensitive to the error resulting from misalignment of the transducer with respect to the ship's gyrocompass. Because we are calculating relative rather than absolute velocities, this error is small—proportional to the relative current times the sine of the misalignment angle.

In estimating the error in the ADCP transport, we assumed that inertial waves were the largest scale coherent flow. Therefore, the inertial length/time scale is the minimum horizontal/temporal averaging scale for estimating the Ekman transport. The inertial period at 11°N is 63 h, and each CTD station interval was

about 6 hours or 10% of the local inertial period. We have thus approximately eight inertial periods in our section; one period corresponds to a steaming distance of 500 km. The vertically integrated transport was calculated over each 500 km segment. Then, omitting the eastern most and western most segments (the former because of the anomalously low wind stress and the latter due to the strong boundary current), the remaining six were treated as independent realizations of ADCP transport. The sample standard deviation is 1.9 Sv, and the standard error of the total ADCP transport, the sum of eight such segments, is 5.4 Sv.

By assuming that T^g and T^d are independent and normally distributed random variables, we can compute the standard deviation of the difference variable and find 5.5 Sv for the error estimate of the total ageostrophic transport.

We do not believe that the in situ wind measurements are representative of time-averaged conditions; in view of the observed variability between legs they clearly are not. The standard error estimate is the error of estimating the wind-driven transport from this single section. It was determined in a manner analogous to that used for the ADCP transport. Wind-derived transports over the same six 500 km intervals along the ship track were used to estimate the variance of the large-scale wind (standard deviation of 0.67 Sv). The error estimate in the sum, the net wind-derived transport, is 1.9 Sv.

The error of the transport computed from the climatology was the standard error of the transport summation, assuming each $2 \times 2°$ box was an independent estimate (21 independent values used), and using the standard error maps presented by HR. The resulting error in the net transport was 0.3 Sv. A more realistic error estimate, based on uncertainties in drag coefficient and on systematic observation errors is likely to be several Sv but is quite difficult to assess.

REFERENCES

Chereskin, T. K., M. D. Levine, A. J. Harding and L. A. Regier, 1989: Observations of near-inertial waves in acoustic Doppler current profiler measurements made during MILDEX. *J. Geophys. Res.*, **94,** 8135–8145.

Davis, R. E., R. deSzoeke and P. P. Niiler, 1981: Variability in the upper ocean during MILE. Part II: Modeling the mixed layer response. *Deep-Sea Res.*, **28A,** 1453–1475.

D'Asaro, E. A., 1984: Wind forced internal waves in the north Pacific and Sargasso Sea. *J. Phys. Oceanogr.*, **14,** 781–794.

Ekman, V. W., 1905: On the influence of the earth's rotation on ocean-currents. *Ark. Mat. Astron. Fys.*, **2,** 1–52.

Hellerman, S., and M. Rosenstein, 1983: Normal monthly wind stress over the world ocean with error estimates. *J. Phys. Oceanogr.*, **13,** 1093–1104.

Kaufeld, L., 1981: The development of a new Beaufort equivalent scale. *Meteorol. Rundsch.*, **34,** 17–23.

Kosro, P. M., 1985: Shipboard acoustic current profiling during the Coastal Ocean Dynamics Experiment. Ph.D. thesis, SIO Ref 85-8, Scripps Institution of Oceanography, 119 pp.

Large, W. G., and S. Pond, 1981: Open ocean momentum flux measurements in moderate to strong winds. *J. Phys. Oceanogr.*, **11,** 324–336.

Leaman, K. D., and T. B. Sanford, 1975: Vertical energy propagation of inertial waves: a vector spectral analysis of velocity profiles. *J. Geophys. Res.*, **80,** 1975–1978.

Pollard, R. T., 1977: Obervations and models of the structure of the upper ocean. *Modelling and Prediction of the Upper Layers of the Ocean,* E. B. Kraus, Eds., Pergamon, pp. 102–117.

——, and J. Read, 1989: A method for calibrating shipmounted acoustic Doppler profilers and the limitations of gyro compasses. *J. Atmos. Oceanic Technol.*, **6,** 859–865.

Price, J. F., R. A. Weller and R. R. Schudlich, 1987: Wind-driven ocean currents and Ekman transport. *Science,* **238,** 1534–1538.

Roemmich, D., 1983: The balance of geostrophic and Ekman transports in the tropical Atlantic ocean. *J. Phys. Oceanogr.*, **13,** 1534–1539.

——, 1989: Mean transport of mass, heat, salt and nutrients in southern California coastal waters: implications for primary production and nutrient cycling. *Deep-Sea Res.*, **36,** 1359–1377.

Weller, R. A., 1981: Observations of the velocity response to wind forcing in the upper ocean. *J. Geophys. Res.*, **86,** 1969–1977.

Wyrtki, K., 1981: An estimate of equatorial upwelling in the Pacific. *J. Phys. Oceanogr.*, **11,** 1205–1214.